Available online at www.sciencedirect.com
ScienceDirect
Trans. Nonferrous Met. Soc. China 28(2018) 1687−1694
Transactions of Nonferrous Metals Society of China
www.tnmsc.cn

Nucleation potency prediction of LaB_6 with E2EM model and its influence on microstructure and tensile properties of Al−7Si−0.3Mg alloy

Li-jun JING[1], Ye PAN[1], Tao LU[1,2], Jin-hong PI[2], Teng-fei GU[1]

1. Jiangsu Key Laboratory of Advanced Metallic Materials, School of Materials Science and Engineering, Southeast University, Nanjing 211189, China;
2. Jiangsu Key Laboratory of Advanced Structural Materials and Application Technology, Nanjing Institute of Technology, Nanjing 211167, China

Received 18 July 2017; accepted 28 December 2017

Abstract: The edge-to-edge matching (E2EM) crystallographic model was used to predict the orientation relationships (ORs) between LaB_6 and Al. Three different possible ORs can be predicted between LaB_6 and Al, which are $(100)_{Al}||(100)_{LaB_6}$, $[001]_{Al}||[001]_{LaB_6}$; $(110)_{Al}||(110)_{LaB_6}$, $[001]_{Al}||[001]_{LaB_6}$; and $(111)_{Al}||(111)_{LaB_6}$, $[01\bar{1}]_{Al}||[01\bar{1}]_{LaB_6}$. The prediction results are perfectly confirmed through TEM analysis and prove the nucleation potency of LaB_6. The refining efficacy of Al−2La−1B refiner and its influence on the tensile properties were investigated in the as-cast Al−7Si−0.3Mg alloy. According to the results, LaB_6 has higher nucleation potency than TiB_2, leading to better grain refining efficacy of Al−2La−1B refiner in the as-cast Al−7Si−0.3Mg alloy. Regarding the mechanical performances, tensile properties of the as-cast Al−7Si−0.3Mg casting alloy are prominently improved after addition of Al−2La−1B refiner, due to the refined microstructures.

Key words: edge-to-edge matching; orientation relationship; casting aluminum alloy; grain refinement; tensile properties

1 Introduction

Grain refinement is a practical method to improve mechanical properties and metallurgical quality of aluminum castings [1−4]. Although many new techniques, such as electromagnetic vibrational method [5] and rapid solidification [6,7], have been developed, chemical inoculation of grain refiner is still the best cost-effective method for the refinement of grain structure of aluminum alloys during the solidification processes [8]. Although there is much argument about the refinement mechanism, two factors are believed to play important roles in grain refinement. One is the nucleant particles existing in grain refiners, e.g., Al_3Ti [9], TiB_2 [10], AlB_2 [2] and TiC [11], inducing the heterogeneous nucleation process, and the other is the growth restriction factor caused by constitutional undercooling [12,13].

The edge-to-edge matching (E2EM) model, which is reported by ZHANG and KELLY [14,15], is based on the matching of rows of atoms across the interface. It is capable of predicting the orientation relationships (ORs) and the corresponding habit plane with matrix from the first principles, and therefore can be directly applied to new alloy development. The E2EM model has been applied to the typical grain refiners in aluminum alloys [16]. According to the results, there are four different ORs between Al_3Ti and Al, more than three Ors of TiC and two Ors of Ti or AlB_2, indicating that Al_3Ti is a more powerful nucleating substrate for primary Al than TiC, TiB_2 and AlB_2. This agrees with previous experimental results and shows that E2EM model has the potential to be a powerful tool in discovering new and more powerful grain refiners for Al alloys [16].

Although Al_3Ti is a more powerful nucleating substrate for wrought aluminum, when applied to casting alloy which contains more than 4% silicon element, it exhibits lower refining efficiency for primary Al because of poisoning phenomenon between Ti and Si [17]. More recently, grain refiners with lower mass ratios of Ti to B have been applied in Al−Si foundry alloys [17].

Foundation item: Project (BM2007204) supported by Jiangsu Key Laboratory for Advanced Metallic Materials, China; Project (ASMA201501) supported by the Opening Project of Jiangsu Key Laboratory of Advanced Structural Materials and Application Technology, China
Corresponding author: Ye PAN, Tel: +86-25-52090681, E-mail: panye@seu.edu.cn; Tao LU, E-mail: lutao@seu.edu.cn
DOI: 10.1016/S1003-6326(18)64812-5

These master alloys contain TiB_2 other than Al_3Ti, as a consequence, they perform better refining efficiency than Al−5Ti−1B in Al−Si casting alloys. Previous works [18,19] have illustrated that LaB_6, a simple cubic structure crystal, owns small crystal lattice mismatch with α(Al) phase and can refine the grain structures of pure aluminum. However, it is still confused whether LaB_6 can act as more effective nucleating substrate than TiB_2. Up to now, a few investigations have been devoted to the refining effect of LaB_6 in Al−Si alloys. Therefore, it is significant to compare the nucleation potency between LaB_6 and TiB_2 with guidance of E2EM model and evaluate their grain refinement efficacy in Al−Si alloys.

In the present work, E2EM model is applied to calculating the ORs between LaB_6 and Al. TEM analysis is utilized to confirm the calculation results. Considering that the mass ratio of La to B in LaB_6 is 2:1 and Ti to B in TiB_2 is 2.2:1, two kinds of master alloys, Al−2La−1B and Al−2.2Ti−1B were prepared. The grain refining efficiencies of Al−2La−B and Al−2.2Ti−1B are investigated in Al−7Si−0.3Mg alloy, respectively. The influence of master alloy additions on mechanical properties and the fractographs of tensile samples are also studied.

2 Experimental

2.1 Alloy preparation

The master alloys and Al−7Si−0.3Mg alloy were both prepared in a graphite crucible using electric resistance furnace. The Al−2La−1B master alloy was prepared with commercial pure aluminum, Al−10La and Al−3B master alloys. The Al−2.2Ti−1B master alloy was obtained by Halide Salt process [15]. The starting materials were pure aluminum(99.7% Al), and K_2TiF_6 and KBF_4 salt of commercial purity. The Al−7Si−0.3Mg alloy was melted with commercial pure aluminum, magnesium and A413.0 alloy. When studying the transformation of microstructure and tensile properties of Al−7Si−0.3Mg alloy, grain refiners were added into the melt when the temperature was brought to (720±5) °C. The melts (720±5) °C were poured into ASTM: B−108 type permanent mold preheated to (250±5) °C to produce tensile test bars.

2.2 Characterizations

The grain refining performance of grain refiners was evaluated by samples solidified in a cylindrical graphite mould (d25 mm × 100 mm) surrounded by refractory brick. The cast samples were sectioned 25 mm from the bottom surface. The samples were anodized in Barker's solution and then examined with an optical microscope under polarized light. The grain sizes were measured with the linear intercept method.

The chemical compositions of the samples were analyzed with optical emission spectroscopy (OES) (Table 1). The original alloy (Al−7Si−0.3Mg without inoculation) was labeled as S0, after adding 0.25%, 0.5%, 0.75% and 1.0% Al−2.2Ti−1B, 0.25%, 0.5%, 0.75% and 1.0% Al−2La−1B, the experimental alloys were labeled as S1−S8, respectively. For more obvious contrast, when analyzing the nucleation potency and fractographs, only S0, S2, S4, S6 and S8 alloys were compared. The phase composition was characterized by means of X-ray diffraction (D8-Discover, Bruker, Germany). The morphology of the particles in the prepared sample was observed by scanning electron microscope (SEM, Sirion, FEI) equipped with energy dispersive X-ray spectrometer (EDX). Transmission electron microscopy (TEM) analysis was used to discover the crystalline orientation relationship between LaB_6 and α(Al), which was performed on a Tecnai G2 instrument. The samples for TEM analysis were fabricated by focused ion beam (FIB, Helios nanolab 600, FEI) machine. The tension testing was conducted on a mechanical testing machine (CMT5105, SANS), according to ASTM: B557−2010 standard.

Table 1 Chemical composition of Al−7Si−0.3Mg alloy in present work (mass fraction, %)

Sample	Si	Mg	Fe	La	Ti	B	Al
S0	7.13	0.325	0.0865	0.0005	0.0013	0.0006	Bal.
S1	7.06	0.338	0.0765	0.0005	0.0060	0.0031	Bal.
S2	7.01	0.341	0.0821	0.0005	0.0130	0.0067	Bal.
S3	7.22	0.309	0.0663	0.0005	0.0171	0.0080	Bal.
S4	6.86	0.351	0.0733	0.0006	0.0215	0.0105	Bal.
S5	6.97	0.329	0.0739	0.0063	0.0012	0.0032	Bal.
S6	7.09	0.337	0.0773	0.0105	0.0011	0.0055	Bal.
S7	7.31	0.316	0.0768	0.0176	0.0013	0.0082	Bal.
S8	7.23	0.355	0.0875	0.0221	0.0010	0.0138	Bal.

3 Results and discussion

3.1 E2EM model calculation

The E2EM model was utilized to predict the orientation relationships between LaB_6 and Al. The crystal structure and lattice parameters of LaB_6 and Al are listed in Table 2. The interatomic spacing misfit (f_r) and interplanar spacing mismatch (f_d) between LaB_6 and Al are calculated by the following equations:

$$f_r = \frac{|r_s - r_c|}{r_c} \quad (1)$$

$$f_d = \frac{|d_s - d_c|}{d_c} \quad (2)$$

where r_s and r_c are the atomic linear densities of close packed or nearly close packed directions of substrate and Al matrix without deformation, respectively; d_s and d_c are the interplanar distance of close packed or nearly close packed planes of substrate and Al matrix, respectively.

Al matrix is a simple FCC structure, and the lattice parameter a is 0.4049 nm. There are three possible close packed or nearly close packed directions in Al crystal. They are $\langle 110\rangle_{Al}$, $\langle 100\rangle_{Al}$ and $\langle 112\rangle_{Al}$ [16]. LaB_6 (JSPDF No. 65−1831) is simple cubic structure, CsCl type and belongs to $Pm\bar{3}m$ space group [20]. The lattice parameter a of LaB_6 is 0.4157 nm. There are three possible close packed directions, $\langle 100\rangle_{LaB6}$, $\langle 110\rangle_{LaB6}$ and $\langle 111\rangle_{LaB6}$ (Table 2). Because each phase has three possible close or nearly close packed directions, there are nine direction pairs. Table 3 lists the calculated misfits along these nine direction pairs. It can be seen that there are two direction pairs, $\langle 100\rangle_{Al}/\langle 100\rangle_{LaB6}$ and $\langle 110\rangle_{Al}/\langle 110\rangle_{LaB6}$, of which the f_r is 2.67%, less than 10%. Hence, $\langle 100\rangle_{Al}/\langle 100\rangle_{LaB6}$ and $\langle 110\rangle_{Al}/\langle 110\rangle_{LaB6}$ are potential matching directions.

The second step in the prediction of the orientation relationships is to examine the d-value mismatch between the possible matching planes. The close and nearly close packed planes for Al are $\{111\}_{Al}$, $\{200\}_{Al}$ and $\{220\}_{Al}$, which contain $\langle 001\rangle_{Al}$ and $\langle 011\rangle_{Al}$ directions (Fig. 1). The close and nearly close packed planes for LaB_6 are $\{110\}_{LaB6}$, $\{100\}_{LaB6}$ and $\{111\}_{LaB6}$, which contain $\langle 001\rangle_{LaB6}$ and $\langle 011\rangle_{LaB6}$ directions (Fig. 2). As each phase has three close or nearly close packed planes, there will also be nine possible plane pairs. The d-value mismatch of these nine plane pairs is listed in Table 4. From Table 4 we can see the possible matching planes. They are $\{200\}_{Al}/\{100\}_{LaB6}$, $\{220\}_{Al}/\{110\}_{LaB6}$ and $\{111\}_{Al}/\{111\}_{LaB6}$, the mismatches of which are all 2.67%, less than 6%. The final orientation relationships between LaB_6 and Al matrix are predicted as follows:

$(100)_{Al}\|(100)_{LaB_6}$, $[001]_{Al}\|[001]_{LaB_6}$;

$(110)_{Al}\|(110)_{LaB_6}$, $[001]_{Al}\|[001]_{LaB_6}$;

$(111)_{Al}\|(111)_{LaB_6}$, $[01\bar{1}]_{Al}\|[01\bar{1}]_{LaB_6}$

3.2 TEM demonstration

For verifying the above calculation results, the TEM analysis was employed to identify the crystallographic relationship between LaB_6 and Al in S6 alloy (Fig. 3). LaB_6 particle locating in the center of α(Al) is contained in the TEM foil sample (Fig. 3(a)). LaB_6 phase shows typical facet morphology located in the Al matrix (Figs. 3(b) and (c)). Figure 3(f) shows the overlapping SAED pattern of LaB_6 (Fig. 3(d)) and Al matrix

Table 2 Crystal structure, close-packed rows and close-packed planes of α(Al) and LaB_6

Sample	Structure	a/nm	CP row	d_{uvw}/nm	CP plane	d_{hkl}/nm
Al	FCC	0.405	⟨110⟩	0.286	{200}	0.202
			⟨100⟩	0.405	{220}	0.143
			⟨112⟩	0.496	{111}	0.234
LaB_6	Cubic	0.416	⟨110⟩	0.588	{110}	0.294
			⟨100⟩	0.416	{100}	0.416
			⟨111⟩	0.720	{111}	0.240

Table 3 Interatomic spacing misfit (relative to Al) along possible matching directions between LaB_6 (a=0.416 nm) and Al matrix (a=0.405 nm)

a_{LaB_6}/nm	f_r/%								
	$[110]_{Al}/[100]_{LaB_6}$	$[110]_{Al}/[110]_{LaB_6}$	$[110]_{Al}/[111]_{LaB_6}$	$[100]_{Al}/[100]_{LaB_6}$	$[100]_{Al}/[110]_{LaB_6}$	$[100]_{Al}/[111]_{LaB_6}$	$[112]_{Al}/[100]_{LaB_6}$	$[112]_{Al}/[110]_{LaB_6}$	$[112]_{Al}/[111]_{LaB_6}$
0.416	45.2	2.7[a]	45.2	2.7	45.2	77.8	16.1	18.5	45.2

[a] indicates that two interatomic spacings in Al match one spacing in LaB_6

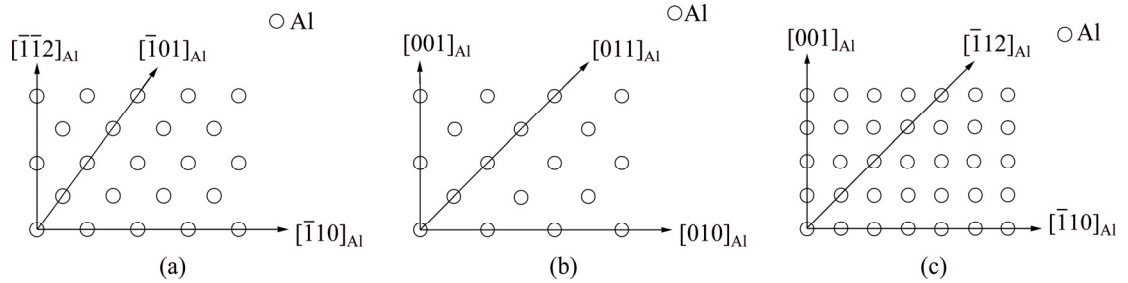

Fig. 1 Atom configuration of Al on three possible close packed planes: (a) $(111)_{Al}$; (b) $(200)_{Al}$; (c) $(220)_{Al}$

Table 4 Interplanar spacing mismatch (relative to Al) between close or nearly close packed planes in LaB_6 (a=0.416nm) and Al matrix (a=0.405 nm)

a_{LaB6}/nm	f_r/%								
	$(200)_{Al}$/ $(110)_{LaB_6}$	$(200)_{Al}$/ $(100)_{LaB_6}$	$(200)_{Al}$/ $(111)_{LaB_6}$	$(220)_{Al}$/ $(110)_{LaB_6}$	$(220)_{Al}$/ $(100)_{LaB_6}$	$(220)_{Al}$/ $(111)_{LaB_6}$	$(111)_{Al}$/ $(110)_{LaB_6}$	$(111)_{Al}$/ $(100)_{LaB_6}$	$(111)_{Al}$/ $(111)_{LaB_6}$
0.416	−27.4[a]	2. 7[a]	−40.7[a]	2.7[a]	45.2[a]	−16.1[a]	25.7	77.8	2.7

[a] indicates that two interplanar spacings in Al match one interplanar spacing in LaB_6

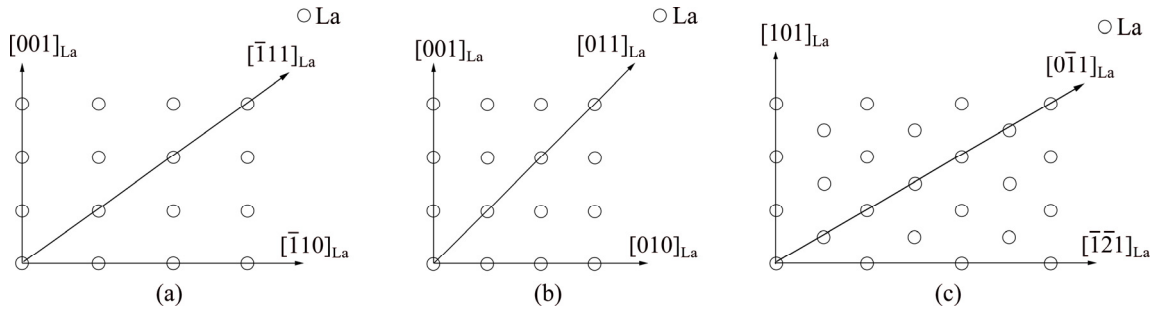

Fig. 2 Atom configuration of LaB_6 on three possible close packed planes: (a) $(110)_{La}$; (b) $(100)_{La}$; (c) $(111)_{La}$

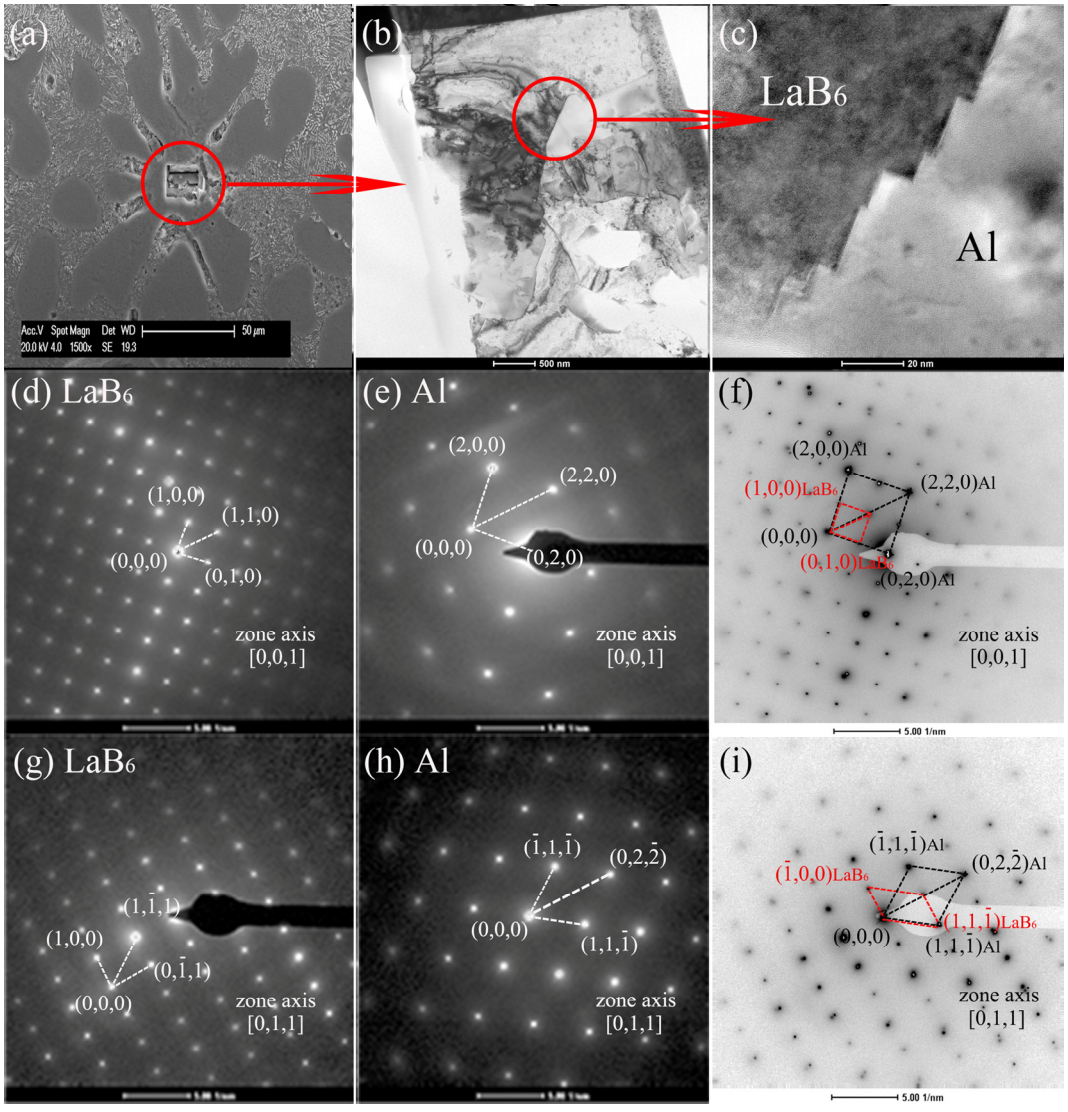

Fig. 3 TEM analysis of LaB_6 existing in center of α(Al): TEM images of location of sample (a), foil sample (b) and region around interface between LaB_6 and Al (c), and corresponding SAED patterns of LaB_6 particle (d, g), and Al matrix (e, h), and overlapping of SAED pattern of LaB_6 and Al (f, i)

(Fig. 3(e)) with the zone axis [001]. It is shown that $(100)_{Al}$ is nearly parallel to $(100)_{LaB_6}$ and $(110)_{Al}$ is also parallel to $(110)_{LaB_6}$. From this point of view, the crystalline orientation relationships $(100)_{Al}||(100)_{LaB_6}$, $[001]_{Al}||[001]_{LaB_6}$ and $(110)_{Al}||(110)_{LaB_6}$, $[001]_{Al}||[001]_{LaB_6}$ do exist between LaB_6 and Al. It can also be seen in Fig. 3(i) that $(111)_{Al}$ is parallel to $(111)_{LaB_6}$ with the zone axis [011], then the third orientation relationship $(111)_{Al}||(11\bar{1})_{LaB_6}$, $[011]_{Al}||[01\bar{1}]_{LaB_6}$ is obtained. Hence, three orientation relationships are observed between LaB_6 and Al, which are consistent with the calculation results by E2EM model. In comparison to the ORs between TiB_2 and Al, which are $(200)_{Al}||(10\bar{1}1)_{TiB2}$, $[011]_{Al}||[1\bar{2}10]_{TiB_2}$ and $(220)_{Al}||(11\bar{2}0)_{TiB_2}$, $[\bar{1}12]_{Al}||[1\bar{1}00]_{TiB_2}$, respectively, LaB_6 possesses more ORs with Al matrix, indicating higher grain refining efficacy, according to the theory of ZHANG et al [16].

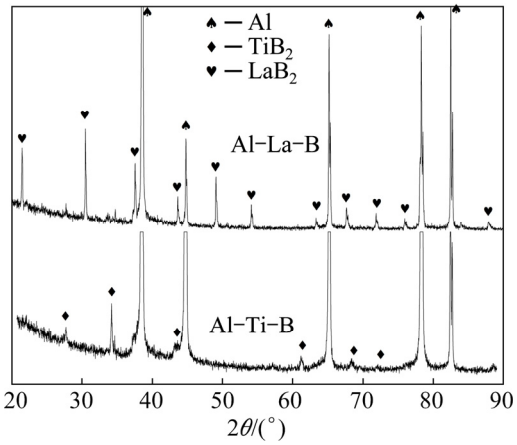

Fig. 4 XRD patterns of Al−2La−1B and Al−2.2Ti−1B master alloys

3.3 Microstructure evolution

To demonstrate the prediction result, Al−2La−B and Al−2.2Ti−1B master alloys were added into Al−7Si−0.3Mg alloy, respectively, and then the grain refining efficacy was compared.

Firstly, phases and microstructures of Al−2La−B and Al−2.2Ti−1B master alloys were analyzed by XRD and SEM, respectively. According to the results of XRD analysis (Fig. 4), the Al−2La−B and Al−2.2Ti−1B master alloys are both dual-phase. There are LaB_6 and Al in Al−2La−B and TiB_2 and Al in Al−2.2Ti−1B master alloys, respectively. The morphologies of particles in two kinds of master alloys are shown in Fig. 5. In consideration of EDS results, the bright phase in Al−2La−B master alloy is regarded as LaB_6, of which the mean particle size is approximately 2 μm. The bright particles in Al−2.2Ti−1B master alloy are considered as TiB_2, the mean particle size of which is smaller than LaB_6.

Figure 6 illustrates the microstructures of Al−7Si−0.3Mg alloys inoculated with different master alloys. It is clear that, with inoculations, grain of S0 alloy is refined in different degrees. The mean grain sizes of the samples with different master alloys are shown in Fig. 7. The mean grain size of original alloy S0 is in average 1190 μm. After adding 0.5% Al−La−B master alloy, the mean grain size reduced dramatically to about 430 μm, less than that of 631 μm in the S2 alloy. When the addition level is more than 0.75%, the variation of mean grain size of Al−7Si−0.3Mg alloy is not significant. Obviously, both LaB_6 and TiB_2 particles can act as the

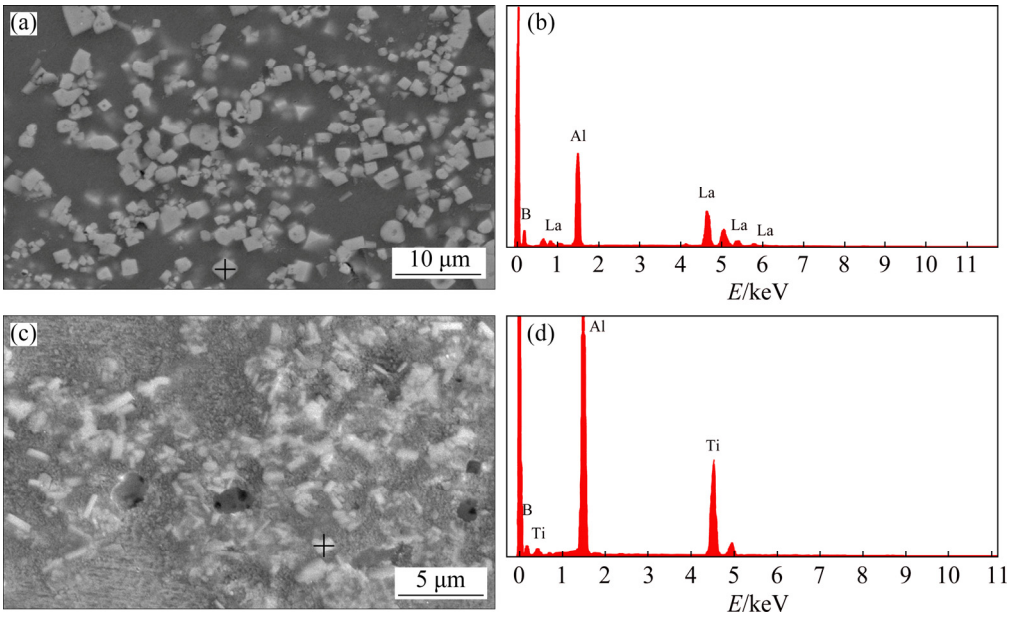

Fig. 5 SEM images (a, c) and EDS spectra (b, d) of LaB_6 particles in Al−2La−1B master alloy (a, b) and TiB_2 particles in Al−2.2Ti−1B master alloy (c, d)

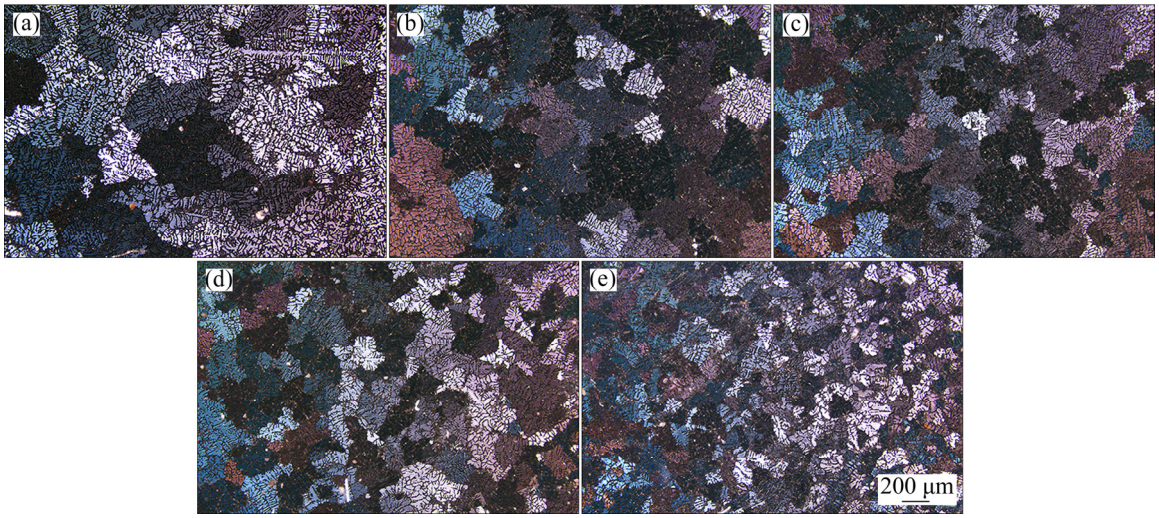

Fig. 6 Grain structures of Al−10Si−0.3Mg alloy before and after grain refinement with different master alloys: (a) Without inoculation; (b) 0.5% Al−Ti−B; (c) 1.0% Al−Ti−B; (d) 0.5% Al−La−B; (e) 1.0% Al−La−B

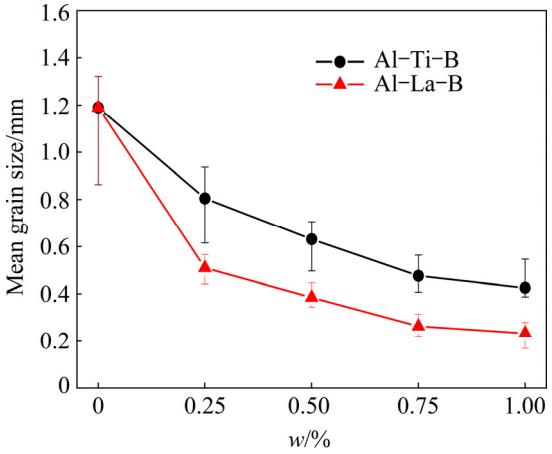

Fig. 7 Mean grain sizes of samples with different addition levels of Al−2La−1B and Al−2.2Ti−1B master alloys

substrate of α(Al), which significantly increases the nucleation rate to induce the grain refinement. Moreover, the mean grain sizes of alloys inoculated with Al−2La−B are smaller than that of alloys refined by Al−2.2Ti−1B master alloy, under the same mass ratio addition. It can be concluded that the Al−2La−B master alloy performs higher refinement efficacy in Al−7Si−0.3Mg.

3.4 Tensile properties

To further analyze the improvement of tensile properties of Al−7Si−0.3Mg alloy with inoculation by Al−2La−B and Al−2.2Ti−1B master alloys, the ultimate strength and elongation with different addition levels of master alloys are tested (Fig. 8). Owing to grain refinement, the as-cast tensile properties of Al−7Si−0.3Mg are improved with the increase of master alloys. With the same addition, the tensile properties of the alloy inoculated by Al−2La−B master alloy are higher than that of alloy refined by Al−2.2Ti−1B master alloy, which

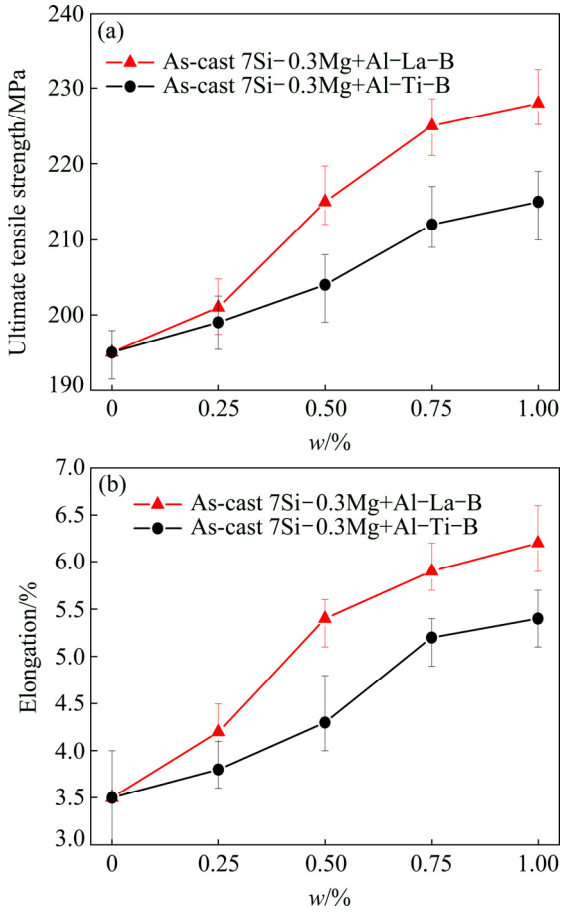

Fig. 8 Tensile properties of Al−7Si−0.3Mg alloy with different addition levels of master alloys: (a) Ultimate tensile strength; (b) Elongation

is in accordance with the results of grain refinement. Figure 9 shows fractographs of each tensile samples. In S0 alloy, the fracture surface displays a mixed quasi-cleavage and dimple morphology. With the inoculation

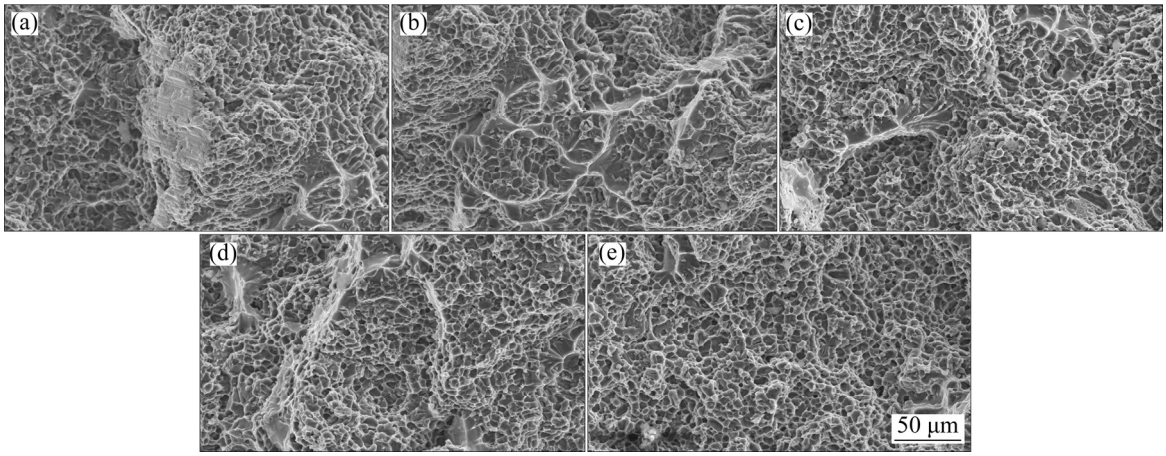

Fig. 9 SEM fractographs of alloys: (a) Without inoculation; (b) 0.5% Al−Ti−B; (c) 1.0% Al−Ti−B; (d) 0.5% Al−La−B; (e) 1.0% Al−La−B

of master alloys, the fracture surfaces are transformed to complete dimple fracture. In the alloy inoculated by Al−2La−B master alloy (S6 and S8), the smaller and deeper dimples with high density uniformly distribute on the fracture surface, leading to the simultaneous enhancement of UTS and elongation.

4 Conclusions

1) Three different possible ORs can be predicted between LaB_6 and Al, calculated by E2EM model, which are $(100)_{Al}||(100)_{LaB_6}$, $[001]_{Al}||[001]_{LaB_6}$; $(110)_{Al}||(110)_{LaB_6}$, $[001]_{Al}||[001]_{LaB_6}$; and $(111)_{Al}||(111)_{LaB_6}$, $[01\bar{1}]_{Al}||[01\bar{1}]_{LaB_6}$, which are confirmed by TEM analysis. The results indicate that LaB_6 has higher nucleation potency than TiB_2. The grain refining efficacy of Al−2La−B master alloy is apparently better than that of Al−2.2Ti−1B master alloy in Al−7Si−0.3Mg alloy.

2) With the inoculation of master alloys, the as-cast tensile properties of Al−7Si−0.3Mg alloy are improved obviously. In comparison to Al−2.2Ti−1B, the same addition of Al−2La−B master alloy leads to a higher tensile property in Al−7Si−0.3Mg alloy, which is consistent with the results of grain refinement. With LaB_6 inoculation, the smaller and deeper dimples with high density uniformly distribute on the fracture surface, leading to the simultaneous enhancement of UTS and elongation.

References

[1] EASTON M A, QIAN M, PRASAD A, STJOHN D H. Recent advances in grain refinement of light metals and alloys [J]. Current Opinion in Solid State & Materials Science, 2016, 20: 13−24.

[2] BIROL Y. Grain refining AlSi7Mg0.3 foundry alloy with commercial Al−4B master alloy [J]. Materials Science and Technology, 2014, 30: 465−470.

[3] LI Hong-ying, LI De-wang, ZHU Zhi-xiang. Grain refinement mechanism of as-cast aluminum by hafnium [J]. Transactions of Nonferrous Metals Society of China, 2016, 26: 3059−3069.

[4] CAMICIA G, TIMELLI G. Grain refinement of gravity die cast secondary AlSi7Cu3Mg alloys for automotive cylinder heads [J]. Transactions of Nonferrous Metals Society of China, 2016, 26: 1211−1221.

[5] MIZUTANI Y, TAMURA T, MIWA K. Effect of electromagnetic vibration frequency and temperature gradient on grain refinement of pure aluminum [J]. Materials Transactions, 2007, 48: 538−543.

[6] LI Guo-cong, MA Yue, HE Xiao-lei. Damping capacity of high strength-damping aluminum alloys prepared by rapid solidification and powder metallurgy process [J]. Transactions of Nonferrous Metals Society of China, 2012, 22: 1112−1117.

[7] BROCHU M, PORTILLO G. Grain refinement during rapid solidification of aluminum−zirconium alloys using electrospark deposition [J]. Materials Transactions, 2013, 54: 934−939.

[8] SIGWORTH G K, KUHN T A. Grain refinement of aluminum casting alloys [J]. International Journal of Metalcasting, 2007, 1: 31−40.

[9] CIBULA A. The mechanism of grain refinement of sand castings in aluminium alloys [J]. Journal of the Institute of Metals, 1949, 76: 321−325.

[10] KUMAR G S V, MURTY B S, CHAKRABORTY M. Settling behaviour of TiAl3, TiB2, TiC and AlB2 particles in liquid Al during grain refinement [J]. International Journal of Cast Metals Research, 2010, 23: 193−204.

[11] DING W, ZHAO W, XIA T. Grain refining action of Al−5Ti−C and Al−TiC master alloys with Al−5Ti master alloy addition for commercial purity aluminium [J]. International Journal of Cast Metals Research, 2014, 27: 187−192.

[12] QUESTED T E, GREER A L. Grain refinement of Al alloys: Mechanisms determining as-cast grain size in directional solidification [J]. Acta Materialia, 2005, 53: 4643−4653.

[13] QUESTED T E, GREER A L. Athermal heterogeneous nucleation of solidification [J]. Acta Materialia, 2005, 53: 2683−2692.

[14] ZHANG M X, KELLY P M. Edge-to-edge matching and its applications - Part I. Application to the simple HCP/BCC system [J]. Acta Materialia, 2005, 53: 1073−1084.

[15] ZHANG M X, KELLY P M. Edge-to-edge matching and its applications - Part II. Application to Mg−Al, Mg−Y and Mg−Mn alloys [J]. Acta Materialia, 2005, 53: 1085−1096.

[16] ZHANG M X, KELLY P M, EASTON M A, TAYLOR J A. Crystallographic study of grain refinement in aluminum alloys using

the edge-to-edge matching model [J]. Acta Materialia, 2005, 53: 1427−1438.

[17] BIROL Y. Performance of AlTi5B1, AlTi3B3 and AlB3 master alloys in refining grain structure of aluminium foundry alloys [J]. Materials Science and Technology, 2012, 28: 481−486.

[18] LI P T, LI C, NIE J F, OUYANG J, LIU X F. Growth and design of LaB6 microcrystals by aluminum melt reaction method [J]. Crystengcomm, 2013, 15: 411−420.

[19] CHEN Y, PAN Y, LU T, TAO S W, WU J L. Effects of combinative addition of lanthanum and boron on grain refinement of Al-Si casting alloys [J]. Materials & Design, 2014, 64: 423−426.

[20] LI P T, TIAN W J, WANG D, LIU X F. Grain refining potency of LaB_6 on aluminum alloy [J]. Journal of Rare Earths, 2012, 11: 1172−1176.

使用 E2EM 模型预测 LaB6 的形核潜力及其对 Al−7Si−0.3Mg 合金组织和拉伸性能的影响

景力军[1]，潘 冶[1]，陆 韬[1,2]，皮锦红[2]，顾腾飞[1]

1. 东南大学 材料科学与工程学院 先进金属材料实验室，南京 211189；
2. 南京工程学院 江苏先进结构材料和应用技术实验室，南京 211167

摘 要：采用边−边匹配模型预测 LaB_6 与 Al 之间的位向关系。预测结果显示 LaB_6 与 Al 之间存在 3 种不同的位向关系，分别为$(100)_{Al}\|\|(100)_{LaB_6}$，$[001]_{Al}\|\|[001]_{LaB_6}$；$(110)_{Al}\|\|(110)_{LaB_6}$，$[001]_{Al}\|\|[001]_{LaB_6}$和$(111)_{Al}\|\|(111)_{LaB_6}$，$[01\bar{1}]_{Al}\|\|[01\bar{1}]_{LaB_6}$。TEM 分析结果完美地证明了模型的预测结果并证明了 LaB_6 的形核潜力。研究 Al−2La−B 细化剂在 Al−7Si−0.3Mg 合金中的细化效率及其对合金性能的影响。根据结果可知，LaB_6 比 TiB_2 拥有更高的形核潜力，这使 Al−2La−1B 细化剂在 Al−7Si−0.3Mg 合金中表现出更好的细化效果。在合金性能方面，由于添加细化剂后的组织得到改善，Al−7Si−0.3Mg 合金的拉伸性能显著提高。

关键词：边−边匹配；位向关系；铸造铝合金；晶粒细化；拉伸性能

(Edited by Xiang-qun LI)